REGULAR ARTICLE



Plasmonic Phenomena in Metallic Nanocap

R.Yu. Korolkov¹, R.O. Malysh¹, V.I. Reva¹, A.V. Korotun¹,²,* ⊠ ଢ, N.V. Shyrokobokova¹, V.V. Shyrokobokov¹

¹ Zaporizhzhia Polytechnic National University, 69011 Zaporizhzhia, Ukraine
 ² G.V. Kurdyumov Institute for Metal Physics, N.A.S. of Ukraine, 03142 Kyiv, Ukraine

(Received 20 August 2025; revised manuscript received 20 October 2025; published online 30 October 2025)

The optical properties of the composite nanostructure based on the spherical dielectric particle incompletely covered by the metallic shell (nanocap) have been investigated. The expressions for the diagonal components of the polarizability tensor, absorption, scattering and extinction cross-sections, and radiation efficiency are obtained. The methodology for determining the transverse and longitudinal effective relaxation rates is proposed. The frequencies of the transverse and longitudinal surface plasmonic resonances are obtained within the framework of the hybridization of the modes of the elementary (simplest) forms of the plasmonic nanostructures - the metallic segment and the dielectric cavity in metal. The frequency dependences of the real and imaginary parts, as well as the modulus of the diagonal components of the polarizability tensor, absorption, scattering and extinction cross-sections, and radiation efficiency have been calculated. The qualitative similarity and quantitative proximity of the corresponding curves for the transverse and longitudinal polarizabilities have been established. It is shown that the amplitude, spectral position and number of maxima of the absorption, scattering and extinction cross-sections essentially depend on the geometrical parameters of the nanostructure, and the maxima at some resonance frequencies are not visually observed due to the smallness of their amplitude. The influence of the geometrical parameters, core and shell material properties on the position and amplitude of the maxima of the extinction cross-section is investigated. The simpler scheme of the hybridization of the plasmonic modes, based on the Drude model, conditions of the absence of the energy losses and excitation of the transverse and longitudinal plasmonic surface resonances, is developed. This scheme differs from the scheme, which is used in the number of the known works. An increase in the splitting of the longitudinal and transverse surface plasmonic resonances with increasing volume content of the dielectric in the nanostructure is proved. The growth of the radiation efficiency of the nanostructures, which are under the study, with increasing content of the metallic fraction in them is demonstrated.

Keywords: Metallic nanocap, Polarizability tensor, Surface plasmonic resonance, Radiation efficiency, Absorption, Scattering and extinction cross-sections, Effective relaxation rate.

DOI: 10.21272/jnep.17(5).05022 PACS numbers: 78.67.Bf, 78.67.Pt, 79.60.Jv

1. INTRODUCTION

The metal-dielectric nanostructures are important components of the optical and optoelectronic devices, including, logic circuits [1-6], sensors and structures for energy conversion [7-10]. In the nanoscale devices, the optical characteristics depend on the geometry of their subwavelength components, usually metallic structures, which determine the ability to control and manipulate light. As the electrical connections approach the fundamental quantum limit with decreasing size, the metallic plasmonic nanostructures become an alternative replacement for the traditional embedded connections [11, 12]. By focusing light in the volume much smaller than the diffraction limit, plasmonic nanostructures make it possible to create the subwavelength optical components with the size of modern integrated logical microcircuits [11, 13].

It is known that the plasmonic properties of the complex nanostructures can be explained within the

framework of the hybridization model of the plasmonic modes of their elementary constituents [14], the paradigm that provides the possibility of predicting plasmonic characteristics [15]. Many of the unique electromagnetic properties of the complex metallic nanostructures arise when their symmetry is reduced. For example, it has been shown that cut ring resonators [16,17] are important components of metamaterials because of their ability to support the magnetic resonances at microwave frequencies, since such materials will have the negative permeability in this spectral range.

The family of the metallic nanoshells provides several routes to the nanostructures of the reduced symmetry with the unique optical properties in the visible and near-infrared regions of the spectrum. The spherical nanoparticles, consisting of the dielectric core and the metallic shell, support the surface plasmonic resonances that can be tuned to wavelengths ranging from the near ultraviolet to the infrared region of the spectrum [18-26].

2077-6772/2025/17(5)05022(10)

05022 - 1

https://jnep.sumdu.edu.ua

^{*} Correspondence e-mail: andko@zp.edu.ua

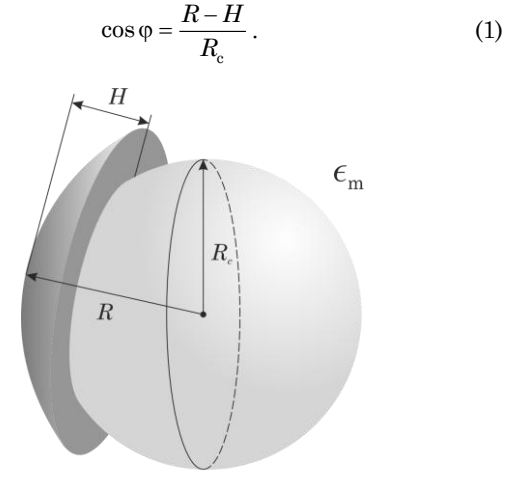
Even more significant changes in the plasmonic properties arise when the morphology of the nanoparticles itself becomes anisotropic. Increasing or decreasing the thickness of one side of the nanoshell leads to the non-concentric displacement of the core with respect to the shell layer, the morphology known as the "nanoegg" [18, 27]. In this geometry, the selection rule that allows plasmonic modes of exclusively the same angular momentum to be mixed is relaxed, leading to new plasmonic resonances in the optical spectrum [18, 27]. At the same time, lowering the symmetry of the metallic nanoshells by cutting out a part of them leads to the series of nanostructures such as "nanocaps", "halfshells" and "nanocups" [28]. The excitation of both electric and magnetic plasmonic modes is possible in the particles with this geometry, with potential applications as the components of the magnetic materials or metamaterials [29, 30]. The nanocaps (or nanocups) exhibit the strong dependence of the optical properties on the angle of the incidence and polarization of the incident light [28, 29]. As a result, the arrays of such particles can serve as the angle and spectrally selective filters [30]. They also significantly enhance the fields at the edge of the shell, which is useful in surface-enhanced Raman spectroscopy (SERS) applications [31].

It should be pointed out that the optical and plasmonic properties of the two-layer spherical, cylindrical and disc nanoparticles were theoretically studied in the works [26, 32-36]. At the same time, the theoretical studies of the optical properties of such objects as the dielectric particle partially covered by the metallic shell are absent in the scientific literature, so this issue is actual.

2. MATHEMATICAL MODEL

2.1 Polarizability Tensor, Absorption, Scattering and Extinction Cross-sections, Radiation Efficiency

Let the spherical dielectric nanoparticle be partially covered by the metallic shell (Fig. 1), and its height H < R, where R is the radius of the whole nanostructure, $R_{\rm c}$ is the radius of the dielectric core, ϕ is the angle, which is determined by the relation



 $\blacksquare \epsilon(\omega) \ \Box \ \epsilon_{c}$

Fig. 1 – Geometry of the problem

The mentioned metal-dielectric nanostructure has been named "nanocap" in the scientific literature.

We consider that the permittivities of the core and ambient materials are equal $\epsilon_{\rm c}$ and $\epsilon_{\rm m}$ respectively. Since the considered nanostructure is axisymmetric, its polarizability is the diagonal tensor of the second rank

$$\alpha_{\hat{e}}^{ij} = \begin{pmatrix} \alpha_{\hat{e}}^{\perp} & 0 & 0\\ 0 & \alpha_{\hat{e}}^{\perp} & 0\\ 0 & 0 & \alpha_{\hat{e}}^{\parallel} \end{pmatrix}, \tag{2}$$

and the relations for the diagonal components of this tensor coincide in form with the relations for the diagonal components of the polarizability tensor of the bilayer spheroidal nanoparticle [35,36]

$$\alpha_{@}^{\perp(\parallel)} = V_0 \frac{\epsilon_{@}^{\perp(\parallel)} - \epsilon_{m}}{\epsilon_{m} + \mathcal{L}_{\perp(\parallel)}^{(2)} \left(\epsilon_{@}^{\perp(\parallel)} - \epsilon_{m}\right)}, \tag{3}$$

where $V_0 = 4\pi R^3/3$, the depolarization factors of the incomplete shell

$$\mathcal{L}_{\parallel}^{(2)} = rac{1}{2} igg(1 - eta_{
m c}^{-1/3} + rac{H}{R_{
m c}} igg), ~~ \mathcal{L}_{\perp}^{(2)} = rac{1}{2} igg(1 - \mathcal{L}_{\parallel}^{(2)} igg), \ (4)$$

and the diagonal components of the dielectric tensor of the structure, which is under the study

$$\epsilon_{@}^{\perp(\parallel)} = \epsilon_{s}^{\perp(\parallel)} \left[1 + \tilde{\beta}_{c} \frac{\epsilon_{c} - \epsilon_{s}^{\perp(\parallel)}}{\epsilon_{s}^{\perp(\parallel)} + \left(\epsilon_{c} - \epsilon_{s}^{\perp(\parallel)}\right) \left(\mathcal{L}_{\perp(\parallel)}^{(1)} - \tilde{\beta}_{c}\mathcal{L}_{\perp(\parallel)}^{(2)}\right)} \right]. \tag{5}$$

In formula (5) $\mathcal{L}_{\perp}^{(1)}=\mathcal{L}_{\|}^{(1)}=1/3\,,$ the bulk content of the dielectric

$$\tilde{\beta}_{c} = \left\{ 1 + \frac{1}{2} \left(\beta_{c}^{-1} - 1 \right) \left(1 + \frac{H}{R_{c}} - \beta_{c}^{-1/3} \right) \right\}^{-1}, \tag{6}$$

 $\beta_c = \left(R_c/R\right)^3$, and the diagonal components of the dielectric tensor of the shell material in Drude model

$$\epsilon_{\rm s}^{\perp(||)}(\omega) = \epsilon^{\infty} - \frac{\omega_p^2}{\omega(\omega + i\gamma_{\rm eff}^{\perp(||)})}.$$
(7)

In formula (7) ϵ^{∞} is the contribution of the crystal lattice into the permittivity; ω_p is plasma frequency, and $\gamma_{\rm eff}^{\perp(\parallel)}$ are the diagonal components of the tensor of the effective relaxation rate, which are going to be determined further.

Knowing the components of the polarizability tensor, one can determine such observable characteristics as the absorption, scattering and extinction cross-sections of the considered nanostructure

PLASMONIC PHENOMENA IN METALLIC NANOCAP

$$\begin{split} C_{@}^{\mathrm{abs}} &= \frac{\omega \sqrt{\epsilon_{\mathrm{m}}}}{c} \operatorname{Im} \left(\frac{2}{3} \alpha_{\perp} + \frac{1}{3} \alpha_{\parallel} \right); \\ C_{@}^{\mathrm{sca}} &= \frac{\omega^{4} \epsilon_{\mathrm{m}}^{2}}{6\pi c^{4}} \left(\frac{2}{3} \left| \alpha_{\perp} \right|^{2} + \frac{1}{3} \left| \alpha_{\parallel} \right|^{2} \right); \\ C_{@}^{\mathrm{ext}} &= C_{@}^{\mathrm{abs}} + C_{@}^{\mathrm{sca}}. \end{split} \tag{8}$$

The radiation efficiency, in turn, is determined by the ratio

$$\xi_{@}^{\text{rad}} = \left(1 + \frac{C_{@}^{\text{abs}}}{C_{@}^{\text{sca}}}\right)^{-1}.$$
 (9)

2.2 Effective Relaxation Rate

The diagonal components of the effective relaxation rate tensor are given by the relations

$$\gamma_{\text{eff}}^{\perp(||)} = \gamma_{\text{bulk}} + \gamma_{\text{s}}^{\perp(||)} + \gamma_{\text{rad}}^{\perp(||)}, \qquad (10)$$

where the additive contributions are determined by the bulk and surface relaxation as well as radiative scattering. Before starting the determination of these contributions, we note an important fact. The results of the calculations will depend on the relations between the angles $\,\phi$ and $\,\theta^*$, where

$$\cos \theta^* = \frac{R_c}{R} = \beta_c^{1/3} \,, \tag{11}$$

and, consequently, on the size relations in the studied nanostructure (Fig. 2), which are determined by the inequalities

$$\begin{cases} 0 < H \le R \left(1 - \frac{R_c^2}{R^2} \right), & 0 < \varphi < \theta^* \qquad \left(\varphi < \theta^* \right); \\ R \left(1 - \frac{R_c^2}{R^2} \right) \le H < R, & \theta^* < \varphi < \frac{\pi}{2} \qquad \left(\varphi > \theta^* \right). \end{cases}$$

$$(12)$$

Let us point out that Fig. 2, a corresponds to the first inequality in (12), and Fig. 2, b corresponds to the second one.

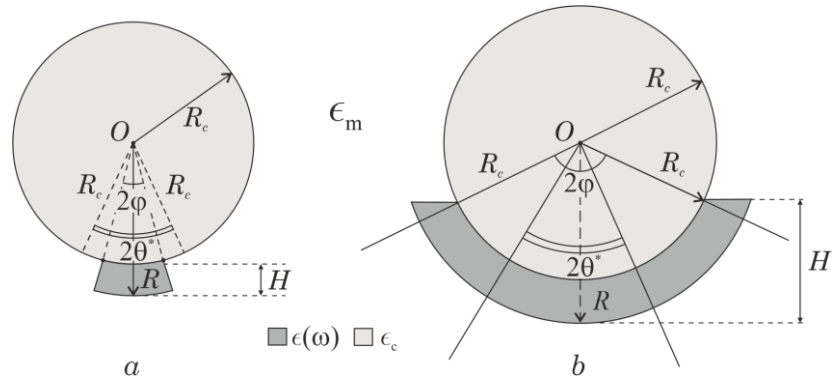


Fig. 2 – Geometries of the nanostructures depending on the relations between the sizes: $a - \varphi < \theta^*$; $b - \varphi > \theta^*$.

In the general case, the bulk relaxation rate and the surface relaxation rate are determined by the expressions

$$\gamma_{\text{bulk}} = \frac{1}{\langle \tau_{\text{bulk}} \rangle},$$
(13)

$$\gamma_{\rm s}^{\perp(\parallel)} = \frac{\upsilon_{\rm F}}{\ell_{\rm off}^{\perp(\parallel)}}, \qquad (14)$$

where $\left\langle \tau_{bulk} \right\rangle$ is the average bulk relaxation time, and $\ell_{eff}^{\perp (\parallel)}$ are the effective free path lengths of electrons in the transverse and longitudinal directions, the general relations for which have the form

$$\ell_{\text{eff}}^{\perp(\parallel)} = \int_{\Omega} L^{\perp(\parallel)}(\theta) \cos \theta d\theta , \qquad (15)$$

and Ω is the range of the angles, which correspond to the inequalities (12).

Let us consider the case when the first inequality from (12) is true:

$$\left\langle \tau_{bulk} \right\rangle = 2 \int\limits_{0}^{\phi} \tau_{s} \cos \theta d\theta = 2 \tau_{s} \sin \phi \; , \label{eq:taubulk}$$

and since $\tau_s=\tau_{bulk}\,,$ then, taking into account expression (1), we have the bulk relaxation rate

$$\gamma_{\text{bulk}} = \frac{1}{2\tau_{\text{bulk}} \sqrt{1 - \left(\beta_{c}^{-1/3} - \frac{H}{R_{c}}\right)^{2}}},$$
 (16)

where $\tau_{\text{bulk}} = \text{const}$ is the bulk relaxation time.

Since

$$L^{\perp}(\theta) = 2R\sin\theta, \qquad L^{\parallel}(\theta) = 2R\left(1 - \beta_{c}^{1/3}\right), \qquad (17)$$

then the effective free path lengths of electrons

$$\ell_{\rm eff}^{\perp} = R \left[1 - \left(\beta_{\rm c}^{-1/3} - \frac{H}{R_{\rm c}} \right)^2 \right],$$
 (18)

R.Yu. Korolkov, R.O. Malysh et al.

$$\ell_{\text{eff}}^{\parallel} = 2R \left(1 - \beta_{\text{c}}^{1/3}\right) \sqrt{1 - \left(\beta_{\text{c}}^{-1/3} - \frac{H}{R_{\text{c}}}\right)^2} \ .$$
 (19)

In the case when the second inequality in (12) is true, the average bulk relaxation time

$$\begin{split} \left\langle \tau_{\text{bulk}} \right\rangle &= \int\limits_{0}^{\theta^{*}} \tau_{\text{s}} \cos \theta d\theta + \int\limits_{\theta^{*}}^{\phi} 2\tau_{\text{s}} \cos \theta d\theta = \\ &= \tau_{\text{s}} \Big(2 \sin \phi - \sin \theta^{*} \Big), \end{split}$$

hence, the bulk relaxation rate

$$\gamma_{\text{bulk}} = \frac{1}{\tau_{\text{bulk}} \left[2\sqrt{1 - \left(\beta_{\text{c}}^{-1/3} - \frac{H}{R_{\text{c}}}\right)^2 - \sqrt{1 - \beta_{\text{c}}^{2/3}}} \right]}.$$
 (20)

Since

$$L^{\perp}(\theta) = \begin{cases} 2R\sin\theta, & 0 < \theta < \theta^*; \\ 2R\left(1 - \beta_c^{1/3}\right), & \theta^* < \theta < \varphi, \end{cases}$$
(21)

then

$$\ell_{\rm eff}^\perp = \int\limits_0^{\theta^*} 2R \sin\theta \cos\theta d\theta + \int\limits_{\theta^*}^{\phi} 2R \Big(1 - \beta_{\rm c}^{1/3}\Big) \cos\theta d\theta \ ,$$

and finally

$$\ell_{\text{eff}}^{\perp} = 2R \left(1 - \beta_{\text{c}}^{1/3} \right) \times \times \left[\frac{1}{2} \left(1 + \beta_{\text{c}}^{1/3} \right) - \sqrt{1 - \beta_{\text{c}}^{2/3}} + \sqrt{1 - \left(\beta_{\text{c}}^{-1/3} - \frac{H}{R_{\text{c}}} \right)^2} \right]. \tag{22}$$

Let us now calculate the effective free path length of electrons in the longitudinal direction.

Since

$$L^{\parallel}(\theta) = \begin{cases} 2R(1 - \beta_{c}^{1/3}), & 0 < \theta < \theta^{*}; \\ 2R\cos\theta, & \theta^{*} < \theta < \varphi, \end{cases}$$
(23)

then

$$\ell_{\rm eff}^{\parallel} = \int\limits_0^{\theta^*} 2R \Big(1 - \beta_{\rm c}^{1/3}\Big) \cos\theta d\theta + \int\limits_{\theta^*}^{\phi} 2R \cos^2\theta d\theta \; , \label{effective}$$

and finally

$$\begin{split} \ell_{\rm eff}^{\parallel} &= R \Bigg[2 \Big(1 - 2 \beta_{\rm c}^{1/3} \Big) \sqrt{1 - \beta_{\rm c}^{2/3}} + \arccos \Bigg(\beta_{\rm c}^{-1/3} - \frac{H}{R_{\rm c}} \Bigg) - \\ &- \arccos \beta_{\rm c}^{1/3} + \Bigg(\beta_{\rm c}^{-1/3} - \frac{H}{R_{\rm c}} \Bigg) \sqrt{1 - \Bigg(\beta_{\rm c}^{-1/3} - \frac{H}{R_{\rm c}} \Bigg)^2} \Bigg]. \end{split} \tag{24}$$

The expressions for the components of the radiation damping rate have the following form in the described above cases:

$$\gamma_{\text{rad}}^{\perp(\parallel)} = \frac{2}{9} \frac{V_0}{\epsilon_m^{1/2}} \left(1 - \tilde{\beta}_c \right) \left(\frac{\omega_p}{c} \right)^3 \times \begin{cases} \gamma_s^{\perp(\parallel)}, & \ell_{\text{bulk}}^s > 2t; \\ \gamma_{\text{bulk}}, & \ell_{\text{bulk}}^s \leq 2t, \end{cases}$$
(25)

where $t=R\left(1-\beta_{\rm c}^{1/3}\right)$ is the thickness of the shell; $\ell_{\rm bulk}^s=v_{\rm F}\tau_{\rm bulk}$, and the expressions for $\gamma_{\rm bulk}$ and $\gamma_{\rm s}^{\perp(||)}$ have the form (16), (14) and (20), and for $\ell_{\rm eff}^{\perp(||)}$ either (18), (19), or (22), (24).

2.3 Hybridization of the Plasmonic Modes

The plasmonic hybridization theory [14] has been developed to understand the plasmonic response of the multilayer metal-dielectric nanoparticles. In this theory, the plasmonic response can be explained in terms of the interactions between the plasmons of the nanostructures in their simplest forms, similar to the way chemical bonding theory explains the formation of the molecular orbitals from the atomic orbitals. For example, the plasmonic resonance of the metallic nanoshell can be considered as the result of the interaction between the sphere $|\hbar\omega_a\rangle$ and cavity $|\hbar\omega_c\rangle$ plasmons (Fig. 3, a). The hybridization of the sphere and cavity plasmons creates two new modes of the plasmonic oscillations, namely the loosening mode with higher energy $|\hbar\omega^{+}\rangle$ and the binding mode with lower energy $\left|\hbar\omega^{-}\right\rangle$, corresponding to the antisymmetric and symmetric interactions between the modes $|\hbar\omega_s\rangle$ and $|\hbar\omega_a\rangle$, correspondingly. However, the mathematical model of the plasmonic hybridization, proposed in [14], in our opinion, has a number of disadvantages. Firstly, it does not directly determine the frequencies of the hybrid modes, and secondly, it is difficult to understand and use in practice. Therefore, in [37] the simpler and clearer model was proposed and implemented for the case of the cylindrical shell using the condition of excitation of the surface plasmonic resonances and the Drude model. This approach will be used to study the hybridization of the plasmonic modes in the nanocap.

Due to the symmetry breaking, instead of one binding dipole resonance, two different binding dipole resonances, one parallel to the symmetry axis (usually called the longitudinal mode) and one perpendicular to the symmetry axis (usually called the transverse mode), arise in the asymmetric nanoshell.

For the nanostructure considered in this work, by analogy with the case of the spherical metallic nanoshell, the simplest forms of the plasmonic nanostructures are the metallic segment and the spherical dielectric cavity in metal, and the longitudinal and transverse plasmonic resonances of the metallic nanocap can be considered as the result of the interaction between the plasmons of the metallic segment $\left|\hbar\omega_s^{\perp(\parallel)}\right\rangle$ and the dielectric cavity in metal $\left|\hbar\omega_c\right\rangle$ (Fig's. 3, b and 3, c).

It is clear that this approach is valid in the absence of damping ($\gamma_{\rm eff}^{\perp(||)}=0$). In this case from the formula (7) follows

$$\epsilon_{sp}^{\perp(\parallel)} \equiv \epsilon_{s}^{\perp(\parallel)} \left(\alpha_{sp}^{\perp(\parallel)} \right) = \epsilon^{\infty} - \frac{\omega_{p}^{2}}{\omega_{sp}^{\perp(\parallel) 2}} . \tag{26}$$

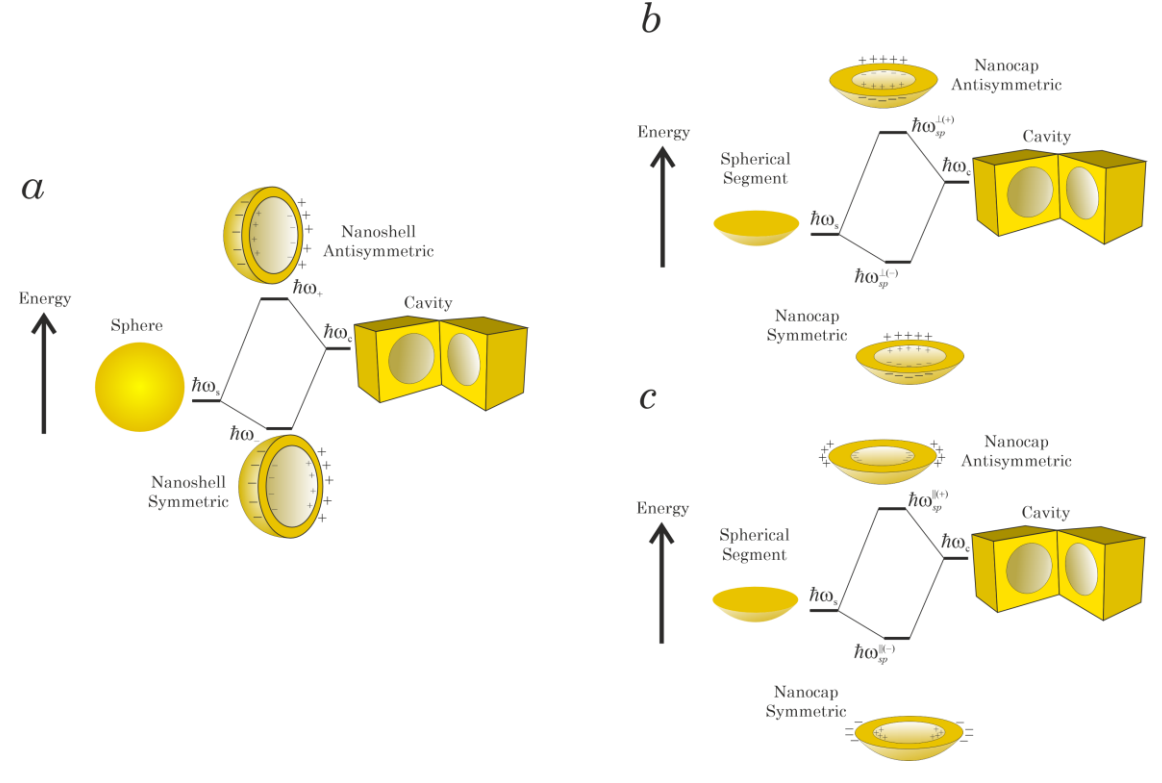


Fig. 3 – The scheme of the energy diagram of the inner Au core and the outer nanocap depicting the plasmonic hybridization: a – the complete shell; b – the longitudinal mode in the nanocap; c – the transverse mode in the nanocap

Then, since the condition of the excitation of the surface plasmonic resonances is equality to zero of the denominator of expression (3), we obtain

taking into account formulas (5) and (27), we have the following quadratic equation for $\epsilon_{sn}^{\perp(|||)}$

$$\epsilon_{@}^{\perp(||)} = -\frac{1 - \mathcal{L}_{\perp(||)}^{(2)}}{\mathcal{L}_{\perp(||)}^{(2)}} \epsilon_{\mathrm{m}},$$
(27)

$$\begin{split} \left[1-\mathcal{L}_{\perp(||)}^{(1)}-\tilde{\beta}_{c}\left(1-\mathcal{L}_{\perp(||)}^{(2)}\right)\right] &\epsilon_{\mathit{sp}}^{\perp(||)\,2} + \left[\left(\mathcal{L}_{\perp(||)}^{(1)}+\tilde{\beta}_{c}\left(1-\mathcal{L}_{\perp(||)}^{(2)}\right)\right) \epsilon_{c} + \frac{1-\mathcal{L}_{\perp(||)}^{(2)}}{\mathcal{L}_{\perp(||)}^{(2)}} \left(1-\mathcal{L}_{\perp(||)}^{(1)}+\tilde{\beta}_{c}\mathcal{L}_{\perp(||)}^{(2)}\right) \epsilon_{m}\right] \epsilon_{\mathit{sp}}^{\perp(||)} + \\ &+ \frac{1-\mathcal{L}_{\perp(||)}^{(2)}}{\mathcal{L}_{\perp(||)}^{(2)}} \left(\mathcal{L}_{\perp(||)}^{(1)}-\tilde{\beta}_{c}\mathcal{L}_{\perp(||)}^{(2)}\right) \epsilon_{c} \epsilon_{m} = 0. \end{split} \tag{28}$$

The solutions of the equation (28) have the form

 $\epsilon_{sp}^{\perp(||)\,(\pm)} = \frac{-b_{\perp(||)} \pm \sqrt{b_{\perp(||)}^2 - 4a_{\perp(||)}c_{\perp(||)}}}{2a_{\perp(||)}} \,, \tag{29}$

where

$$\begin{split} a_{\perp(||)} &= 1 - \mathcal{L}_{\perp(||)}^{(1)} - \tilde{\beta}_{c} \left(1 - \mathcal{L}_{\perp(||)}^{(2)} \right); \\ b_{\perp(||)} &= \left(\mathcal{L}_{\perp(||)}^{(1)} + \tilde{\beta}_{c} \left(1 - \mathcal{L}_{\perp(||)}^{(2)} \right) \right) \epsilon_{c} + \\ &+ \frac{1 - \mathcal{L}_{\perp(||)}^{(2)}}{\mathcal{L}_{\perp(||)}^{(2)}} \left(1 - \mathcal{L}_{\perp(||)}^{(1)} + \tilde{\beta}_{c} \mathcal{L}_{\perp(||)}^{(2)} \right) \epsilon_{m}; \\ c_{\perp(||)} &= \frac{1 - \mathcal{L}_{\perp(||)}^{(2)}}{\mathcal{L}_{\perp(||)}^{(2)}} \left(\mathcal{L}_{\perp(||)}^{(1)} - \tilde{\beta}_{c} \mathcal{L}_{\perp(||)}^{(2)} \right) \epsilon_{c} \epsilon_{m}, \end{split}$$
(30)

or finally

$$\omega_{sp}^{\perp(||)\,(\pm)} = \omega_p \left\{ \epsilon^{\infty} + \frac{b_{\perp(||)} \mp \sqrt{b_{\perp(||)}^2 - 4a_{\perp(||)}c_{\perp(||)}}}{2a_{\perp(||)}} \right\}^{-1/2}, \quad (31)$$

In the following, the relations (3), (8), (9) and (28) taking into account formulas (4) - (7), (10) - (14), (16), (18) - (20), (22), (24) - (26) are going to be used for the calculations.

3. RESULTS OF THE CALCULATIONS AND THEIR DISCUSSION

The calculations of the real and imaginary parts, as well as the modulus of the diagonal components of the polarizability tensor, absorption, scattering and extinction cross-sections, and radiation efficiency were carried out for the nanostructures of dielectric core – incomplete

metallic shell (nanocap) of the different sizes, made of different materials and located in Teflon ($\epsilon_{\rm m}=2.3$). The parameters of metals and dielectrics, required for the calculations, are given in Tables 1 and 2.

Table 1 – The parameters of metals (a_0 is the Bohr radius) (see, for example, [26,36] and references therein)

Metals	Value					
	r_s / a_0	m^* / m_e	ϵ^{∞}	$\hbar\omega_p$, eV	$\hbar \gamma_{\rm bulk},{ m eV}$	
Cu	2.11	1.49	12.03	12.6	0.024	
Au	3.01	0.99	9.84	9.07	0.023	
Ag	3.02	0.96	3.7	9.17	0.016	
Pt	3.27	0.54	4.42	15.2	0.069	
Pd	4.00	0.37	2.52	9.7	0.091	

 $\textbf{Table 3}-\textbf{The calculated values of the frequencies of the transverse and longitudinal SPR for the nanostructures } SiO_2@Ag \ \ \textbf{in Teflon}$

$\beta_{\rm c}$	$\tilde{\beta}_{c}$	$\hbar\omega_{sp}^{\perp(+)}$, eV	$\hbar\omega_{sp}^{\perp(-)}$, eV	$\hbar\omega_{sp}^{\parallel(+)}$, eV	$\hbar\omega_{sp}^{\parallel(+)}$, eV
0.01	0.025	4.233	3.002	4.245	3.333
0.02	0.053	4.265	2.995	4.276	3.168
0.03	0.082	4.297	2.968	4.302	3.030
0.04	0.112	4.328	2.930	4.325	2.907
0.05	0.143	4.357	2.888	4.345	2.792
0.06	0.173	4.386	2.844	4.363	2.684
0.07	0.204	4.412	2.798	4.379	2.580
0.08	0.234	4.437	2.751	4.393	2.481
0.09	0.264	4.461	2.704	4.406	2.385

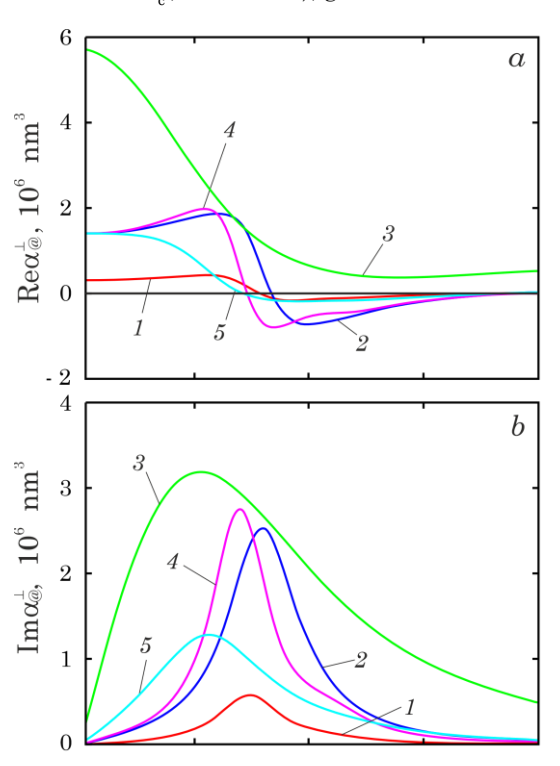
As for the nanostructures of other morphologies in the considered case $\operatorname{Re} \alpha_{@}^{\perp(||)}(\hbar\omega)$ are the alternating functions of frequency, while $\operatorname{Im} \alpha_{\omega}^{\perp(||)}(\hbar\omega) > 0$ in the whole frequency interval, which is under the study. It should be pointed out that the corresponding curves ($\operatorname{Re} lpha_{\scriptscriptstyle{\circledR}}^{\perp}$ and $\operatorname{Re} lpha_{@}^{\parallel}$, $\operatorname{Im} lpha_{@}^{\perp}$ and $\operatorname{Im} lpha_{@}^{\parallel}$, $\left|lpha_{@}^{\perp}\right|$ and $\left|lpha_{@}^{\parallel}\right|$) are qualitatively similar and quantitatively close for the structures of the same sizes. The quantitative difference is that $\operatorname{Re}\alpha_{@}^{\parallel} > \operatorname{Re}\alpha_{@}^{\perp}, \quad \operatorname{Im}\alpha_{@}^{\parallel} > \operatorname{Im}\alpha_{@}^{\perp}, \quad \left|\alpha_{@}^{\parallel}\right| > \left|\alpha_{@}^{\perp}\right|, \quad \text{for the}$ nanostructures of the relatively small sizes (curves 1 in fig. 4, a, b, c and 5, a, b, c), as well as $\max \left\{ \operatorname{Im} \alpha_{@}^{\perp} \right\}$ are achieved at higher frequencies than $\max\{\operatorname{Im}\alpha_{@}^{\parallel}\}$ for the structures of the indicated sizes. In addition, the positions of $\max \left\{ \operatorname{Im} \alpha_{@}^{\perp(||)} \right\}$ depend on the size of the considered nanostructures ($\max \left\{ \operatorname{Im} \alpha_{\scriptscriptstyle \textit{\tiny (I)}}^{\perp (I)} \right\}$ are achieved at both optical frequencies and frequencies from the near ultraviolet range). In this case, the splitting of the frequencies $\omega_{sp}^{\perp(||)}$ on the plots $\operatorname{Im} \alpha_{(a)}^{\perp(||)}(\hbar\omega)$ is not noticeable due to the smallness of the amplitudes of some maxima. Thus, for $\operatorname{Im} \alpha_{\scriptscriptstyle \otimes}^{\parallel}(\hbar\omega)$, only the maxima at frequencies $\omega_{\scriptscriptstyle sn}^{\parallel(-)}$ are noticeable on the plots, while the maxima at frequencies $\omega_{sp}^{\parallel\,(\,+\,)}>\omega_{sp}^{\parallel\,(\,-\,)}\ \ \text{are not noticeable. In turn,}\ \ \max\left\{\operatorname{Im}\alpha_{@}^{\perp}\right\}$ are noticeable both at frequencies $\omega_{sp}^{\perp(+)}$ and $\omega_{sp}^{\perp(-)}$ de-

Table 2 – The permittivities of the core materials [35]

Value	Core					
	SiO_2	$\mathrm{Al}_2\mathrm{O}_3$	ZnO	$\mathrm{Ta_{2}O_{5}}$	$\mathrm{Nb_2O_5}$	
$\epsilon_{ m c}$	2.10	3.10	4.00	4.67	6.15	

The frequency dependences of the real and imaginary parts, as well as the modulus of the transverse and longitudinal components of the polarizability tensor of the structure SiO_2 @Ag under the different values of R_c , R and H, with the height of the nanocap chosen depending on the values R_c and R, according to inequalities (12) are given in Figs. 4 and 5.

pending on the ratio of the radii $R_{\rm c}$ and R, as well as the height of the nanocap H. The mentioned circumstances are confirmed by the results of the direct calculations $\omega_{sp}^{\perp(\pm)}$ and $\omega_{sp}^{\parallel(\pm)}$ at different $\tilde{\beta}_{\rm c}$ (and, respectively, at different $R_{\rm c}$, R and H), given in Table 3.



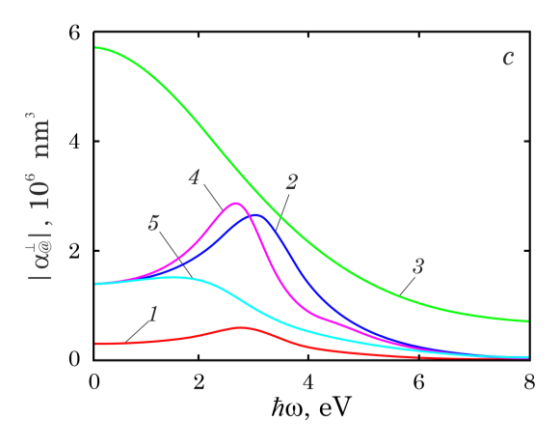


Fig. 4 – The frequency dependencies of the real (a) and imaginary (b) parts, as well as the module (c) of the transverse component of the polarizability tensor of the nanoparticle SiO₂@Ag in Teflon with the different geometric parameters: $1-R_{\rm c}=10\,{\rm nm},\ R=30\,{\rm nm},\ H=25\,{\rm nm};\ 2-R_{\rm c}=10\,{\rm nm},\ R=50\,{\rm nm},\ H=45\,{\rm nm};\ 3-R_{\rm c}=10\,{\rm nm},\ R=80\,{\rm nm},\ H=75\,{\rm nm};\ 4-R_{\rm c}=20\,{\rm nm},\ R=50\,{\rm nm},\ H=40\,{\rm nm};\ 5-R_{\rm c}=25\,{\rm nm},\ R=50\,{\rm nm},\ H=37.5\,{\rm nm}$

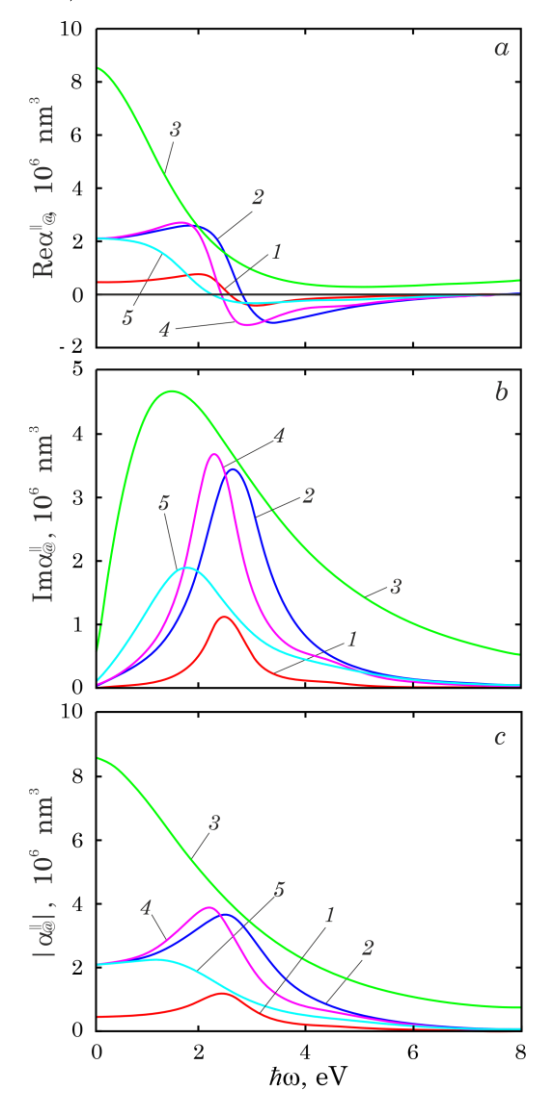


Fig. 5 – The frequency dependencies of the real (a) and imaginary (b) parts, as well as the module (c) of the longitudinal component of the polarizability tensor of the nanoparticle SiO_2 @Ag in Teflon at the same sizes as in Fig. 4

Let us point out that the increase in the content of dielectric in the nanostructure β_c has the consequence of the increase in $\omega_{sp}^{\perp(|||)}(+)$ and decrease in $\omega_{sp}^{\perp(|||)}(-)$, that is, the increase in the splitting of the transverse and longitudinal resonances.

In turn, the behavior of practically all curves (except curve 3) of the frequency dependences of the absorption, scattering and extinction cross-sections are qualitatively similar and quantitatively close (Fig. 6). The above curves (except curve 3 $C_{\tiny @}^{\rm sca}$ and $C_{\tiny @}^{\rm ext}$) have one strongly pronounced maximum at frequencies $\omega_{sp}^{\parallel\,(-)}$ and one weakly pronounced maximum at frequencies $\omega_{sp}^{\perp\,(\pm)}$ (this applies to the nanostructures of those sizes for which $\max\left\{{\rm Im}\,\alpha_{\tiny @}^{\perp}\right\}$ is clearly visible).

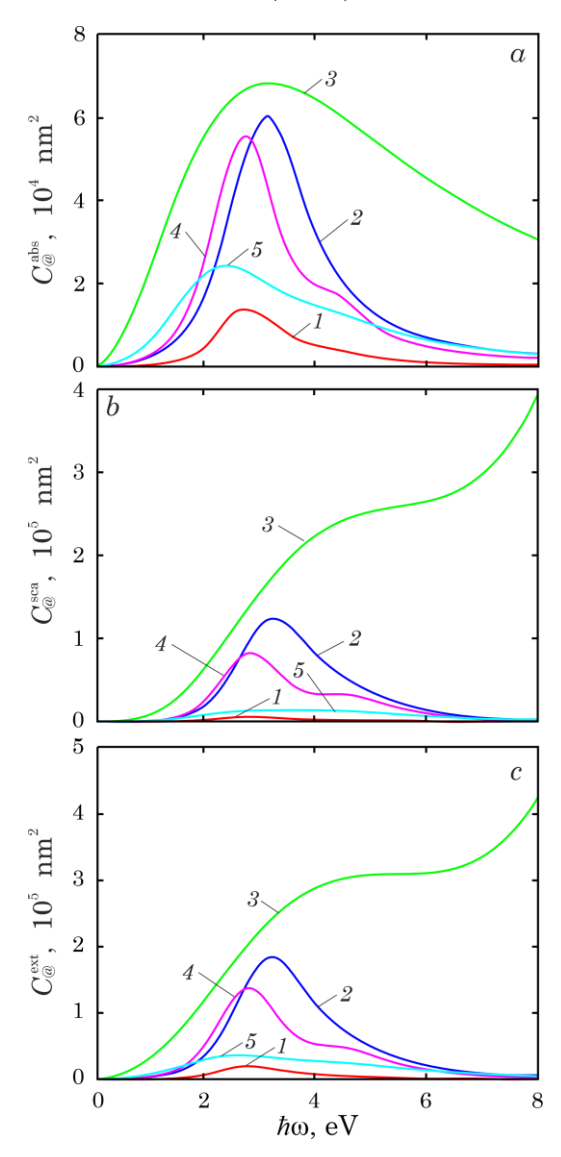


Fig. 6 – The frequency dependencies for the absorption (a), scattering (b) and extinction (c) cross-sections of the nanoparticle $SiO_2@Ag$ in Teflon under the same sizes as in Fig. 4

The frequency dependences of the extinction crosssections at different values of the nanocap height, for

the cases of different shell metals and core dielectrics are given in Fig. 7. The calculation results indicate the presence of "blue" shifts of the first maximum of the extinction cross-section with increasing nanocap height in the sequence of the curves $1 \rightarrow 2 \rightarrow 3 \rightarrow 4 \rightarrow 5$ (increasing bulk content of metal in the nanostructure) and the second maximum in the sequence $1 \rightarrow 2 \rightarrow 3$. At the same time, the curves of the frequency dependencies for the nanocaps of different metals differ significantly. Thus, in the case of Cu, Pd and Pt nanocaps, the corresponding curves have no maximum in the frequency range, which is under the consideration, and are determined by the optical characteristics of these metals. In turn, the change of the dielectric of the core, that is, the decrease in the permittivity in the sequence the dielectrics $\mathrm{Nb_2O_5} \to \mathrm{Ta_2O_5} \to \mathrm{ZnO} \to \mathrm{Al_2O_3} \to \mathrm{SiO_2}$ has a consequence of the weak "blue" shift of both the first and

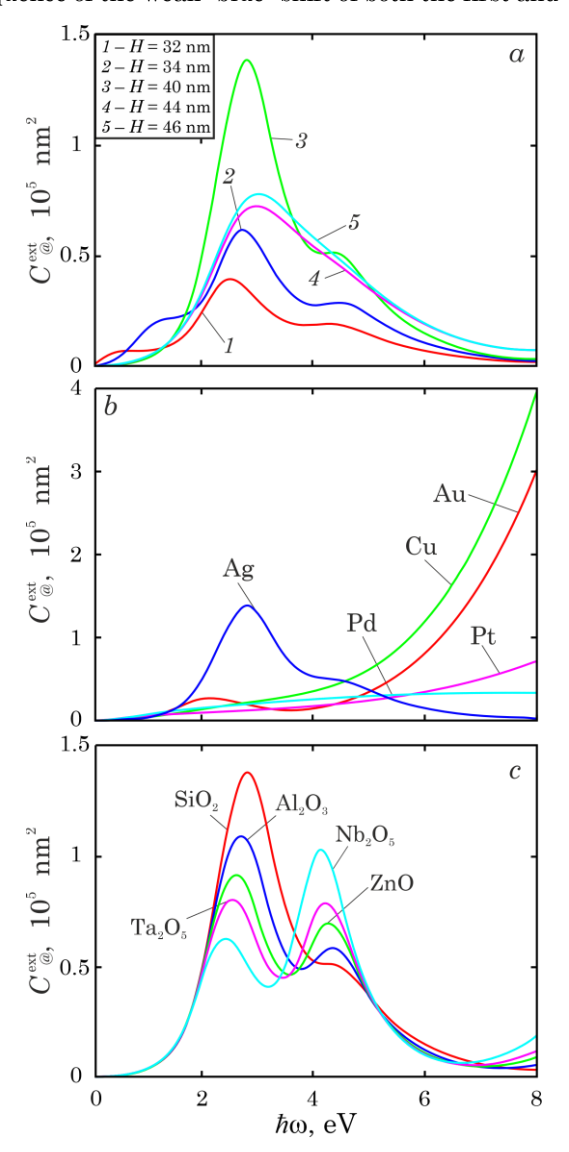


Fig. 7 – The frequency dependencies of the extinction cross-sections for the nanocaps Ag of the different height (a), nanocaps of different metals (b) and nanocaps Ag with the different dielectric core (c) of the constant height $H=40~\rm nm$ under $R_c=20~\rm nm$, $R=50~\rm nm$ in Teflon

second maxima of the extinction cross-section. Let us point out that the increase in the amplitude of the first $\max\left\{C_{@}^{\text{ext}}\right\}$ and the decrease in the amplitude of the second maximum takes place in the same sequence.

The frequency dependences of the radiation efficiency of the considered nanostructures SiO_2 @Ag for the different values of the radius of the core and the whole structure and different values of the nanocap height at constant values of the radii are given in Fig. 8. Since the size parameter β_c decreases for the curves in the sequence $1 \rightarrow 2 \rightarrow 3$ and $5 \rightarrow 4 \rightarrow 3$, the radiation efficiency increases with increasing content of metal in the nanostructures, which are under the study.

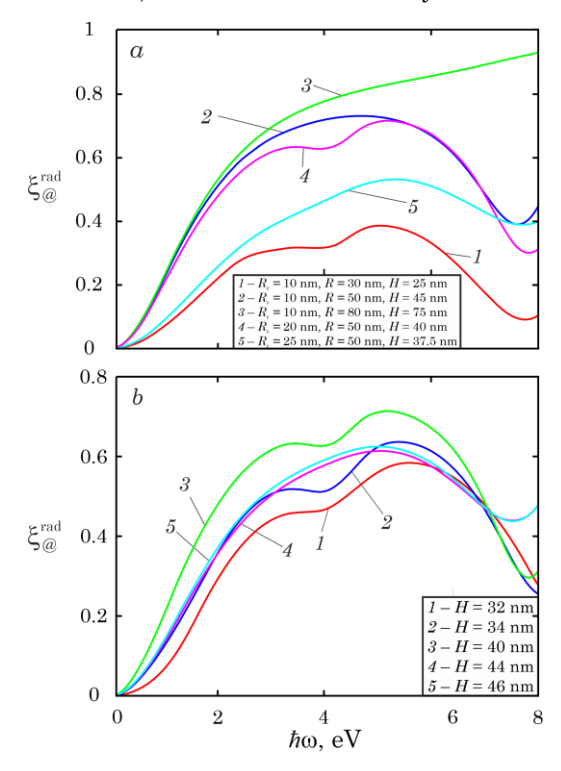


Fig. 8 – The frequency dependencies of the radiation efficiency of the nanocaps ${
m SiO_2}$ @Ag in Teflon under the variation of the radii of the core and the whole structure (a) and the variation of the height of the nanocap under $R_{\rm c}=20~{
m nm}$, $R=50~{
m nm}$ (b)

4. CONCLUSIONS

The relations for the diagonal components of the polarizability tensor, absorption, scattering, and extinction cross-sections, as well as the radiation efficiency of the nanostructures of the "dielectric core — metallic nanocap" type have been obtained.

It is shown that the curves of the frequency dependences of the real and imaginary parts, as well as the modules of the transverse and longitudinal polarizabilities are qualitatively similar and quantitatively close and the maxima of the imaginary parts of the polarizabilities are situated in both visible and near ultraviolet frequency ranges. It was established that the maxima of the imaginary parts of the transverse and longitudinal polarizabilities at some resonance frequencies are not visually

fixed due to their small amplitude.

The increase in the splitting of the resonance frequencies with the increasing dielectric content in the nanostructures, which are under the study, has been proved.

The qualitative similarity of the curves of the frequency dependences of the absorption, scattering and extinction cross-sections is demonstrated. The presence of the well-defined maximum of these dependences at the lower frequency of the longitudinal resonance and the weakly defined maximum at the higher and lower fre-

quencies of the transverse resonance is shown.

The presence of the "blue" shifts of the maxima of the extinction cross-section at increasing the volume content of metal in the nanostructure, which is under the consideration, and decreasing the permittivity of the core material has been established.

The results of the calculations indicate the increase in the radiation efficiency of the nanocaps with increasing bulk content of metal, which is associated with the increase in the scattering cross-section in this case.

REFERENCES

- A.V. Korotun, A.O. Koval, A.A. Kryuchyn, V.M. Rubish, V.V. Petrov, I.M. Titov. Nanophotonic Technologies. Current State and Prospects (Uzhgorod: FOP Sabov A.M.: 2019) (in Ukrainian).
- S.I. Bozhevolnyi, V.S. Volkov, E. Devaux, J.-Y. Laluet, T.W. Ebbesen, *Nature* 440, 508 (2006).
- R. Zia, J.A. Schuller, A. Chandran, M.L. Brongersma, *Mater. Today* 9, 20 (2006).
- T. Holmgaard, Z. Chen, S.I. Bozhevolnyi, L. Markey, A. Dereux, A.V. Krasavin, A.V. Zayats, *Opt. Express* 16, 13585 (2008).
- J.A. Dionne, K. Diest, L.A. Sweatlock, H.A. Atwater, *Nano Lett.* 9, 897 (2009).
- 6. S. Afreen, H.K. Rouf, *Plasmonics* 20, 3905 (2025).
- Y.A. Akimov, W.S. Koh, K. Ostrikov, Opt. Express 17, 10195 (2009).
- S. Pillai, K.R. Catchpole, T. Trupke, M.A. Green, J. Appl. Phys. 101, 093105 (2007).
- M. Schnell, A. García-Etxarri, A.J. Huber, K. Crozier, J. Aizpurua, R. Hillenbrand, Nat. Photonics 3, 287 (2009).
- 10. S. Khani, P. Rezaei, *Heliyon* 10, e40923 (2024).
- 11. E. Ozbay, Science 311, 189 (2006).
- 12. J. Wang, K. Li, Z. Quan, Photonics Insights 3, R05 (2024).
- Q. Zhang, X.-G. Huang, X.-S. Lin, J. Tao, X.-P. Jin, Opt. Express 17, 7549 (2009).
- E. Prodan, C. Radloff, N.J. Halas, P. Nordlander, *Science* 302, 419 (2003).
- H. Wang, D.W. Brandl, P. Nordlander, N.J. Halas, Acc. Chem. Res. 40, 53 (2007).
- S. Linden, C. Enkrich, M. Wegener, J. Zhou, T. Koschny, C.M. Soukoulis, *Science* 306, 1351 (2004).
- N. Liu, H. Guo, L. Fu, S. Kaiser, H. Schweizer, H. Giessen, Nat. Mater. 7, 31 (2008).
- H. Wang, Y. Wu, B. Lassiter, C.L. Nehl, J.H. Hafner,
 P. Nordlander, N.J. Halas, *Proc. Natl. Acad. Sci. U.S.A.* 103, 10856 (2006).

- 19. Y. Wu, P. Nordlander, J. Chem. Phys. 125, 124708 (2006).
- H. Wang, D.W. Brandl, F. Le, P. Nordlander, N.J. Halas, Nano Lett. 6, 827 (2006).
- 21. M. Cortie, M. Ford, Nanotechnology 18, 235704 (2007).
- R. Bukasov, J.S. Shumaker-Parry, *Nano Lett.* 7, 1113 (2007).
- 23. N.A. Mirin, N.J. Halas, Nano Lett. 9, 1255 (2009).
- J. Ye, P. Van Dorpe, W. Van Roy, K. Lodewijks, I. De Vlaminck, G. Maes, G. Borghs, *J. Phys. Chem. C* 113, 3110 (2009).
- 25. V.V. Kulish, J. Nano-Electron. Phys. 3 No 3, 105 (2011).
- A.V. Korotun, A.A. Koval', I.N. Titov, J. Appl. Spectrosc. 87 No 2, 240 (2020).
- R. Malysh, A. Korotun, R. Korolkov, R. Kulykovskyi, 2024 IEEE 42nd International Conference on Electronics and Nanotechnoogy (ELNANO), 191 (Kyiv: 2024).
- 28. M. Cortie, M. Ford, Nanotechnology 18, 235704 (2007).
- J. Ye, L. Lagae, G. Maes, G. Borghs, P. Van Dorpe, Opt. Express 17, 23765 (2009).
- J. Liu, B. Cankurtaran, L. Wieczorek, M.J. Ford,
 M. Cortie, Adv. Funct. Mater. 16, 1457 (2006).
- J. Ye, C. Chen, L. Lagae, G. Maes, G. Borghs, P. Van Dorpe, *Phys. Chem. Chem. Phys.* 12, 11222 (2010).
- A.V. Korotun, A.O. Koval, V.V. Pogosov, *Ukr. J. Phys.* 66 No 6, 518 (2021).
- A.V. Korotun, V.V. Pogosov, Phys. Sol. St. 63 No 1, 122 (2021).
- 34. Y. Karandas, A. Korotun, I. Titov, 2021 IEEE 11th Int. Conf. Nanomaterials: Appl. & Prop. (NAP), 1 (2021).
- 35. Ya.V. Karandas, *Condens. Matter Phys.* **27** No2, 23701 (2024).
- N.I. Pavlyshche, A.V. Korotun, V.P. Kurbatsky, V.I. Reva, Ukr. J. Phys. 70 No4, 263 (2025).
- A.V. Korotun, Y.V. Karandas, *Phys. Met. Metallogr.* 123 No.1, 7 (2022).

Плазмонні явища у металевій нанокришці

Р.Ю. Корольков¹, Р.О. Малиш¹, В.І. Рева¹, А.В. Коротун^{1,2}, Н.В. Широкобокова¹, В.В. Широкобоков

- ¹ Національний університет «Запорізька політехніка», 69011 Запоріжжя, Україна
- ² Інститут металофізики ім. Г. В. Курдюмова НАН України, 03142 Київ, Україна

В роботі досліджено оптичні властивості композитної наноструктури на основі сферичної діелектричної частинки, неповністю вкритої металевою оболонкою (нанокришки). Отримано вирази для діагональних компонентів тензора поляризовності, перерізів поглинання, розсіяння та екстинкції, радіаційної ефективності. Запропоновано методику визначення поперечної та поздовжньої ефективних швидкостей релаксації. Частоти поперечного та поздовжнього поверхневих плазмонних резонансів отримано в рамках уявлень про гібридизацію мод елементарних (найпростіших) форм плазмонних наноструктур — металевого сегмента та діелектричної порожнини в металі. Розраховані частотні залежності дійсної та уявної частин, а також модуля діагональних компонент тензора поляризовності, перерізів поглинання, розсіювання та екстинкції, радіаційної ефективності. Встановлено якісну подібність і кількісну близькість відповідних кривих для поперечної та поздовжньої поляризовностей. По-

казано, що амплітуда, спектральне положення і кількість максимумів перерізів поглинання, розсіювання та екстинкції істотно залежать від геометричних параметрів наноструктури, причому максимуми на деяких резонансних частотах візуально не спостерігаються в силу їх невеликої амплітуди. Досліджено вплив геометричних параметрів, властивостей матеріалів ядра та оболонки на положення та амплітуду максимумів перерізу екстинкції. Розвинено відмінну від використовуваної в низці відомих робіт і більш просту схему гібридизації плазмонних мод, засновану на моделі Друде, умовах відсутності енергетичних втрат і збудження поперечних і поздовжніх плазмонних поверхневих резонансів. Доведено збільшення розщеплення поздовжніх та поперечних поверхневих плазмонних резонансів зі збільшенням об'ємного вмісту діелектрика в наноструктурі. Продемонстровано зростання радіаційної ефективності досліджуваних наноструктур зі збільшенням вмісту в них металевої фракції.

Ключові слова: Металева нанокришка, Тензор поляризовності, Поверхневий плазмонний резонанс, Радіаційна ефективність, Перерізи поглинання, Розсіювання та екстинкції, Ефективна швидкість релаксації.